ISSN 0021-8944, Journal of Applied Mechanics and Technical Physics, 2018, Vol. 59, No. 2, pp. 292–302. © Pleiades Publishing, Ltd., 2018.
Original Russian Text © P. Akbarzadeh, A.H. Fardi.

NATURAL CONVECTION HEAT TRANSFER IN 2D AND 3D TRAPEZOIDAL ENCLOSURES FILLED WITH NANOFLUID

P. Akbarzadeh and A. H. Fardi

UDC 536.223

Abstract: The purpose of the present study is to investigate the heat transfer performance due to free convection of nanofluids with variable properties inside 2D and 3D channels with trapezoidal cross sections. The governing equations are solved numerically using the finite volume method and the SIMPLER algorithm. In this study, the effect of the nanoparticle volume fraction, Rayleigh number, side wall angles of the trapezoidal section, and axial slope of the 3D channel are examined. The presented results include the average Nusselt number, flow circulation streamlines, and isothermal contours. The heat transfer rate (i.e., Nusselt number) is seen to increase in both 2D and 3D channels with an increase in the Rayleigh number. In 2D trapezoidal enclosures, the Nusselt number decreases with an increase in the nanoparticle volume fraction from zero to 2% and increases if the nanoparticle volume fraction is greater than 2%. In 3D channels, an increase in the axial slope of the channel leads to an increase in the Nusselt number.

Keywords: natural convection, nanofluids, inclined 3D trapezoidal enclosure, numerical solution.

DOI: 10.1134/S0021894418020128

INTRODUCTION

Nanofluids are colloids containing metal nanoparticles (Cu, Ag, Al, etc.), metal oxide nanoparticles (CuO, Al_2O_3, TiO_2, etc.), or metallic nanotubes (multi-wall or single-wall nanotubes). The volume fraction of nanoparticles is normally less than 4% of the base fluid. The heat transfer in nanofluids is usually more intense than that in to pure fluids [1]. Results of investigating nanofluid properties find applications in various fields of engineering and are useful for studying various natural phenomena (see, e.g., [2–4]). The existence of some exceptional features in nanofluids, such as thermal conductivity, viscosity, and convective heat transfer coefficient, in comparison with the base fluid has obviously been accepted by many researchers. Clearly, reaching a high Nusselt number and heat transfer enhancement depend on several factors, namely the Brownian motion of nanoparticles, liquid stratification, and nanoparticle clustering [5, 6].

The heat transfer intensity depends on the type of nanofluids, the geometry of enclosures filled by nanofluids, and the boundary conditions. Enclosures of various shapes with different boundary conditions were studied experimentally and numerically by many researchers (see, e.g., [7–16]). In the case of square (or rectangular) enclosures, a detailed comparative numerical study of different models depending on physical properties of nanofluids was performed by Khanafer et al. [9]. In their simulations, a two-dimensional rectangular enclosure was examined by considering a constant temperature for the vertical walls and adiabatic boundary conditions for the top and bottom

Faculty of Mechanical and Mechatronics Engineering, Shahrood University of Technology, Shahrood, Iran; akbarzad@ut.ac.ir; amirhosseinfardi94@gmail.com. Translated from Prikladnaya Mekhanika i Tekhnicheskaya Fizika, Vol. 59, No. 2, pp. 121–133, March–April, 2018. Original article submitted February 20, 2017; revision submitted April 28, 2017.

horizontal walls. They explained that suspended nanoparticles considerably increase the heat transfer rate for any given Grashof number. In addition, they showed that the nanofluid heat transfer rate increases with an increase in the nanoparticle volume fraction. Öğüt [17] studied natural convection of water-based nanofluids (five types of nanoparticles, i.e., Cu, Ag, CuO, Al_2O_3, and TiO_2) in an inclined square enclosure with a heat source (heater) in the middle of the left wall, a constant temperature on the right wall, and an adiabatic boundary condition on the remaining walls. They concluded that the percentage of nanoparticles has a significant impact on the heat transfer rate. The results also illustrated that the heat transfer rate decreases with an increase in the heater length. In addition, they reported that the maximum and minimum heat transfer intensities are observed at enclosure slope angles of 30 and 90°, respectively.

Hu et al. [18] performed experimental and numerical studies of natural convection of Al_2O_3–water nanofluids in a square enclosure with a constant temperature on the vertical walls and an adiabatic boundary condition on the horizontal walls. They concluded that the heat transfer in nanofluids with low nanoparticle concentrations is more sensitive to the thermal conductivity of the nanofluid than to its viscosity. Vice versa, in nanofluids with high nanoparticle concentrations, the heat transfer is more sensitive to the nanofluid viscosity than to its thermal conductivity. Hu et al. [19] conducted experimental and numerical investigations of the natural heat transfer in a square enclosure filled with a TiO_2–water nanofluid. The vertical walls of the enclosure were at a constant temperature, and the horizontal walls were subjected to an adiabatic condition. In that study, they concluded that the heat transfer of the nanofluid at low Rayleigh numbers is more sensitive to an increase in the nanofluid viscosity as compared to an increase in the thermal conductivity. Corcione et al. [20] numerically examined the heat transfer enhancement in a square enclosure filled with water containing CuO, Al_2O_3, or TiO_2 nanoparticles. The left and bottom walls were maintained at a hot temperature, while the top and right walls were cold. They reported that the greatest heat transfer enhancement was observed in the CuO–water nanofluid. They also concluded that the heat transfer increases with an increase in the nanoparticle volume fraction and enclosure width. Bouhalleb and Abbassi [21] studied steady-state natural convection of the CuO–water nanofluid in a rectangular enclosed space heated from one side and cooled from the ceiling. They stated that adding CuO nanoparticles to water leads to heat transfer enhancement. The maximum of this enhancement occurs at the nanoparticle volume fraction of 2% for the aspect ratios of 0.50 and 0.25 and at the nanoparticle volume fraction of 2.5% for the aspect ratios of 0.125, 0.100, and 0.080. Hasan et al. [22] performed some numerical simulations to study the heat transfer enhancement in a square enclosure filled with the Cu–water nanofluid. The bottom wall of the enclosure was kept at a constant hot temperature, while the vertical walls were cold. The top wall moved horizontally with a constant velocity under the adiabatic condition. The heat transfer rate was found to increase with an increase in the Richardson number. Saleh et al. [23] performed a numerical investigation of natural convection inside trapezoidal enclosures filled with water-Cu and Al_2O_3–water nanofluids. In their studies, the left side of the enclosure was at a constant hot temperature and the right side was cold, while the other walls were subjected to an adiabatic condition. They illustrated that the greatest effect on heat transfer enhancement in the case of acutely sloping side walls is observed at high nanoparticle volume fractions. Esfe et al. [24] performed a numerical study of natural convection in a trapezoidal enclosure filled with ethylene glycol–water nanofluid containing carbon nanotubes. The simulation illustrated that conduction heat transfer is dominant at low Rayleigh numbers ($Ra = 10^3$ and 10^4), while convection heat transfer becomes dominant as the Rayleigh number increases. At low Rayleigh numbers ($Ra < 10^4$), the average Nusselt number decreases with increasing inclination angle for all nanoparticle volume fractions. Sheremet et al. [25] conducted a numerical work on steady-state natural convection in a right-angle porous trapezoidal enclosure filled with a nanofluid. The top and bottom walls were subjected to an insulated condition; the right and left side walls were maintained at cold and hot temperatures, respectively. They emphasized that the Nusselt and Sherwood numbers increase with an increase in the Rayleigh number. Hasib et al. [26] performed a numerical study of convection heat transfer in an incompressible nanofluid inside two lid-driven trapezoidal enclosures with different tilt angles. In both enclosures, the top wall was held at a cold temperature and moved with a constant velocity; the down wall was kept at a hot temperature; the other sides were under an adiabatic condition. They concluded that the heat transfer rate increases with increasing tilt angle if the bottom wall is hot. However, if the bottom wall is cold, tilting the enclosure decreases the heat transfer. Nasrin and Parvin [27] performed a numerical study of natural convection heat transfer in a trapezoidal enclosed space filled with a Cu–water nanofluid. In this enclosure, both the top and bottom walls were subjected to an adiabatic condition, while the left and right walls were hot and cold, respectively. They illustrated that the most

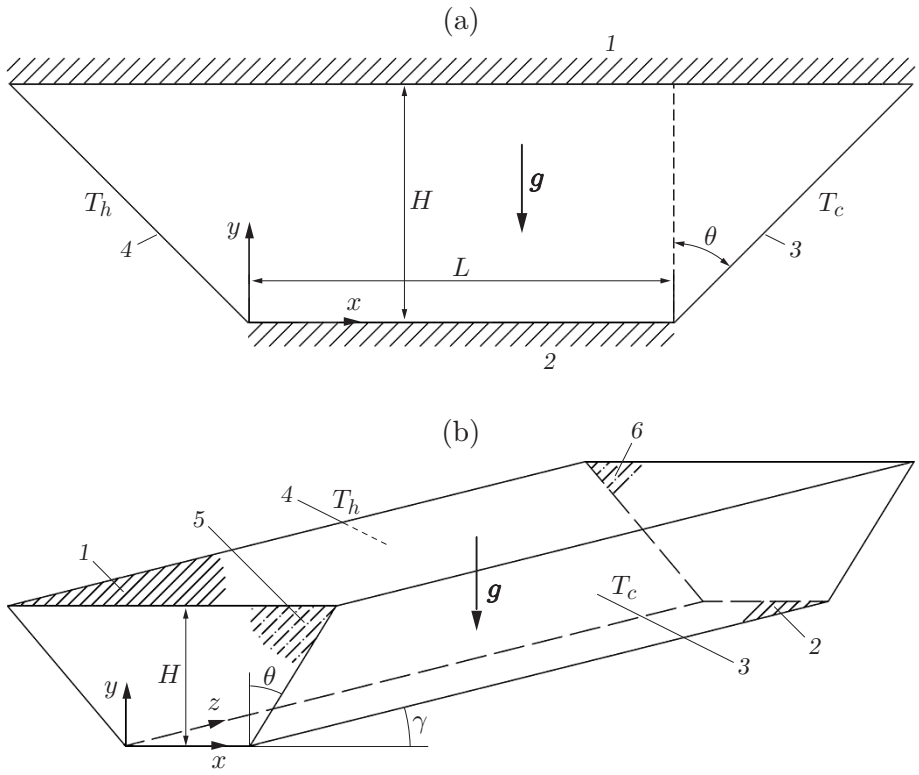

Fig. 1. Geometry of 2D (a) and 3D (b) enclosures: (*1*) insulated top wall; (*2*) insulated bottom wall; (*3*) right wall; (*4*) left wall; (*5*) front face; (*6*) rear face.

intense heat transfer occurs at the lowest aspect ratio (ratio of the base length and height). Mahmoudi et al. [28] investigated entropy generation and heat transfer enhancement for natural convection in a Cu–water nanofluid in the presence of a constant magnetic field. The analysis was performed for a trapezoidal enclosure with a heat flux on the bottom wall. They observed that entropy generation decreases in the presence of nanoparticles, while the magnetic field could increase entropy generation.

The aim of the present paper is to study the heat transfer performance due to natural convection in nanofluids with variable properties inside 2D and 3D channels with trapezoidal cross sections.

1. MODEL AND MATHEMATICS

Figures 1 schematically shows the 2D and inclined 3D trapezoidal enclosures considered in this paper. In both geometries, the left and right side walls are kept hot and cold, respectively, while the adiabatic condition is considered for the top and bottom walls. The velocity components are equal to zero on all solid surfaces because of the no-slip condition and impenetrability of rigid boundaries. The gravity acceleration $\boldsymbol{g}$ is directed downward. The enclosure height H is the characteristic length, L is the base length of the enclosure for both 2D and 3D problems, and θ is the angle of the side wall of the trapezoid for both enclosures. In the 3D enclosure, γ is the angle of the inclined channel. We assume that $A_y = H/L$ and $A_z = b/L$, where b is the depth of the channel in the z direction). If the aspect ratio A_z is large enough, the flow in the channel can be treated by a two-dimensional model. In the 3D problem, it is assumed that $A_z \gg 1$. The natural convective flow occurs in a vertical plane, and the flow velocity vector forms an angle γ with the xy plane. To decrease the computational effort (by considering a channel with a smaller depth and, consequently, fewer grid points), a periodic condition is taken into account for the rear and front faces of the 3D channel. The working fluid in both enclosures is the Al_2O_3–water nanofluid. Its properties for the reference temperature $T_c = 295$ K are described in Table 1 [29, 30]. In the Boussinesq approximation, the

Table 1. Properties of the base fluid and nanoparticles [29, 30] at $T = 22$ °C

Nanofluid component	C_p, J/(kg · K)	ρ, kg/m^3	k, W/(m · K)	$\beta \cdot 10^{-5}$
Water	4179	997.1	0.613	21.00
Nanoparticles Al_2O_3	765	3970.0	40.000	0.85

continuity equation, momentum equations in the x, y, and z directions, and energy equation are written as follows [24, 26–28, 31]:

$$\frac{\partial u}{\partial x} + \frac{\partial v}{\partial y} + \xi \frac{\partial w}{\partial z} = 0,$$

$$\rho_{nf}\Big(u\frac{\partial u}{\partial x} + v\frac{\partial u}{\partial y} + \xi w\frac{\partial u}{\partial z}\Big) = -\frac{\partial p}{\partial x} + \mu_{nf}\Big(\frac{\partial^2 u}{\partial x^2} + \frac{\partial^2 u}{\partial y^2} + \xi\frac{\partial^2 u}{\partial z^2}\Big),$$

$$\rho_{nf}\Big(u\frac{\partial v}{\partial x} + v\frac{\partial v}{\partial y} + \xi w\frac{\partial v}{\partial z}\Big) = -\frac{\partial p}{\partial y} + \mu_{nf}\Big(\frac{\partial^2 v}{\partial x^2} + \frac{\partial^2 v}{\partial y^2} + \xi\frac{\partial^2 v}{\partial z^2}\Big) + g\rho_{nf}\beta_{nf}(T - T_c)\cos\gamma,$$

$$\rho_{nf}\Big(u\frac{\partial w}{\partial x} + v\frac{\partial w}{\partial y} + w\frac{\partial w}{\partial z}\Big) = -\frac{\partial p}{\partial z} + \mu_{nf}\Big(\frac{\partial^2 w}{\partial x^2} + \frac{\partial^2 w}{\partial y^2} + \frac{\partial^2 w}{\partial z^2}\Big) + g\rho_{nf}\beta_{nf}(T - T_c)\sin\gamma, \tag{1}$$

$$u\frac{\partial T}{\partial x} + v\frac{\partial T}{\partial y} + \xi w\frac{\partial T}{\partial z} = \alpha_{nf}\Big(\frac{\partial^2 T}{\partial x^2} + \frac{\partial^2 T}{\partial y^2} + \xi\frac{\partial^2 T}{\partial z^2}\Big).$$

In these equations,

$$\rho_{nf} = (1-\varphi)\rho_f + \varphi\rho_s, \qquad \beta_{nf} = (1-\varphi)\beta_f + \varphi\beta_s,$$

T is the fluid temperature, T_c is the cold temperature, u, v, and w are the velocity components along the x, y, and z axes, respectively, φ is the nanoparticle concentration (or volume fraction), $\alpha_{nf} = k_{nf}/(\rho C_p)_{nf}$ is the thermal diffusivity, $(\rho C_p)_{nf} = (1-\varphi)(\rho C_p)_f + \varphi(\rho C_p)_s$, C_p is the heat capacity, ρ is the density, k is the thermal conductivity, μ is the dynamic viscosity, and β is the expansion coefficient; the subscripts s, f, and nf refer to the solid nanoparticles, base fluid, and nanofluid, respectively.

In system (1), $\xi = 1$ for the 3D problem; for the 2D problem, we have $\xi = \gamma = 0$ and the z momentum equation transforms to an identity.

It should be noted that the viscosity and the thermal conductivity of the nanofluid depend on its temperature and nanoparticle volume fraction. Abu-Nada et al. [32] used the test results of Nguyen et al. [31] and presented a formula for viscosity of the Al_2O_3–water nanofluid:

$$\mu_{Al_2O_3} = \exp\left(3.003 - 0.042\,03T - 0.5445\varphi + 0.000\,255\,3T^2 + 0.0524\varphi^2 - 1.622\varphi^{-1}\right). \tag{2}$$

In Eq. (2), the temperature and viscosity are represented in centigrade degrees and centipoises, respectively. Among many models for calculating the thermal conductivity of nanofluids, such as those derived in [34–36], we chose the model proposed in [36]:

$$k_{nf}/k_f = 1 + 64.7\varphi^{0.7640}(d_f/d_p)^{0.3690}(k_f/k_p)^{0.7476}\mathrm{Pr}_f^{\,0.9955}\,\mathrm{Re}_f^{1.2321}\,.$$

Here $\mathrm{Pr} = \mu/(\rho\alpha)$ is the Prandtl number, $\mathrm{Re} = \rho k_b T/(3\pi\mu^2 l)$ is the Reynolds number, $d_f = 0.384$ nm and $d_p = 47$ nm are the diameters of the fluid molecules and nanoparticles, respectively, $k_b = 1.3807 \cdot 10^{-23}$ is the Boltzmann constant, and $l = 0.17$ nm is the mean free path of fluid particles.

The Rayleigh number $\mathrm{Ra} = g\beta\Delta T H^3/(\alpha\nu)$ is one of the most important dimensionless parameters characterizing the natural convection phenomenon ($\nu = \mu/\rho$ is the kinematic viscosity). This dimensionless number can be defined based on the properties of the pure fluid or based on the nanofluid properties. In this study, we use the nanofluid-based Reynolds number $\mathrm{Ra}_{nf} = g\beta_{nf}\Delta T H^3/(\alpha_{nf}\nu_{nf})$ because the nanofluid properties are temperature-dependent. However, in 3D problems, as the characteristic length changes due to increasing γ, it is necessary to modify the characteristic length by $h = H/\cos\gamma$. Therefore, the Rayleigh number for 3D problems is defined as

$$\mathrm{Ra}_{nf,\gamma} = g\beta_{nf}\Delta T H^3/(\alpha_{nf}\nu_{nf}\cos^3\gamma). \tag{3}$$

The local and average Nusselt numbers are calculated by the formulas

$$\mathrm{Nu} = -\frac{k_{nf}}{k_f}\left.\frac{\partial\tau}{\partial n}\right|_w, \qquad \mathrm{Nu}_{\mathrm{avg}} = \frac{1}{L_w}\int\limits_0^{L_w} \mathrm{Nu}\ dl,$$

where $\tau = (T - T_c)/(T_H - T_c)$ is the dimensionless temperature, n is the direction normal to the solid surface, and L_w is the length of the side walls of the enclosure. The boundary conditions of both 2D and 3D problems are defined as follows:

$T = T_H$ on the left side wall;
$T = T_c$ on the right side wall;
$\partial T/\partial n = 0$ on the top and bottom walls;
$p = 0$ at the bottom left corner;
$u = v = w = 0$ on all walls (no-slip condition).

The following additional conditions are used for the 3D geometry: $(u, v, w, T)_{rf} = (u, v, w, T)_{ff}$ (the subscripts rf and ff refer to the rear and frontal faces, respectively).

2. NUMERICAL METHOD

In this study, the above-formulated boundary-value problem is solved by the finite volume method. A second-order central differencing scheme is used for discretizing the diffusion terms of the energy and momentum equations and a second-order upwind method is utilized for approximating the advective terms. Coupling of the pressure and velocity for the incompressible fluid is achieved by using the well-known Semi-Implicit Method for Pressure-Linked Equations Revised (SIMPLER) [37, 38]. The computational domain is discretized into a structured assembly of tetrahedral elements (four nodes for 2D cases and eight nodes for 3D cases).

3. VALIDATION OF RESULTS

In order to investigate the grid independence of the present simulation, four series of mesh sizes were considered for the 2D and 3D trapezoidal enclosures. Table 2 shows the average Nusselt numbers calculated on the hot wall with different mesh sizes. It is seen that the results for the 2D problem calculated on 80×80 and 160×160 meshes almost coincide with the results for the 3D problem calculated on $80 \times 80 \times 80$ and $160 \times 160 \times 160$ meshes. Therefore, the $80 \times 80 \times 80$ grids and 80×80 grids were selected for 2D and 3D problems, respectively. In addition, for validation of the present solution, the simulation of natural convection of pure water in a 2D square enclosure was compared to the experimental works of [39] and the numerical results of [9]. Figure 2 shows the dimensionless temperature $\tau = (T - T_c)/(T_H - T_c)$ in the mid-section of the enclosure versus the dimensionless coordinate x.

4. RESULTS

For 2D cases, the effects of the Rayleigh number Ra_{nf}, side wall angle θ, and nanoparticle volume fraction φ on the heat transfer rate were considered. For 3D problems, the effects of the Rayleigh number $\mathrm{Ra}_{nf,\gamma}$, slope of the channel over its length γ, and nanoparticle volume fraction φ were examined.

4.1. 2D Enclosure

Let us consider the results of solving 2D and 3D problems. Figure 3 shows the average Nusselt number as a function of the Rayleigh number for different values of the side wall angle θ and nanoparticle volume fraction φ. As the Rayleigh number increases, the average Nusselt number also increases for all values of θ and φ. In fact, with

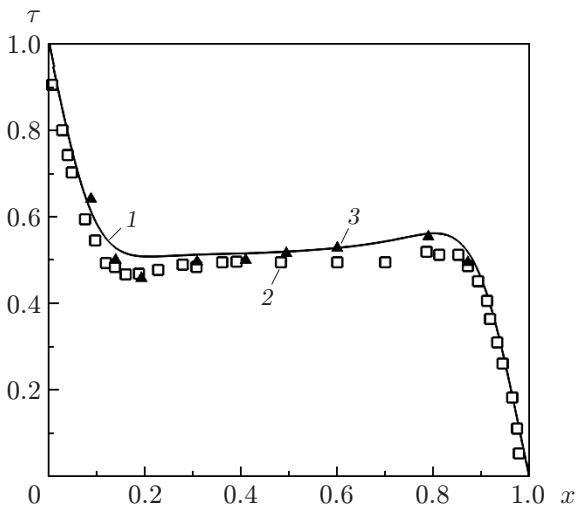

Fig. 2. Dimensionless temperature τ in the enclosure mid-section versus the dimensionless coordinate x for $\mathrm{Ra} = 10^5$ and $\mathrm{Pr} = 0.7$: data of the present work (*1*), data of [9] (*2*), and data of [39] (*3*).

Table 2. Average Nusselt numbers for different side wall angles

Problem geometry	Number of finite elements	$\mathrm{Nu}_{\mathrm{avg}}$		
		$\theta = 30°$	$\theta = 45°$	$\theta = 60°$
2D	20×20	5.60	4.92	3.80
	40×40	5.14	4.49	3.52
	80×80	5.03	4.36	3.44
	160×160	5.00	4.35	3.44
3D ($\gamma = 0°$)	$20 \times 20 \times 20$	2.43	—	—
	$40 \times 40 \times 40$	2.71	—	—
	$80 \times 80 \times 80$	2.94	—	—
	$160 \times 160 \times 160$	2.96	—	—

increasing Rayleigh number, the ratio of the momentum diffusivity to the thermal diffusivity increases, leading to an increase in the natural circulation speed near the hot wall. This velocity increment affects the thermal boundary layer thickness and makes it thinner. Thus, the thermal gradient near the hot wall grows, and the heat transfer is enhanced (the Nusselt number increases).

The effect of the side wall angle θ on the average Nusselt number on the left wall of the enclosure for several values of the Rayleigh number and nanoparticle volume fraction φ is illustrated in Fig. 4. As the side wall angle θ increases, the heat transfer rate (Nusselt number) decreases. At $\theta = 0°$ (enclosure with vertical side walls), the heated fluid remains near the heated wall during its upward motion; consequently, the thermal boundary layer remains thin. As the angle θ increases, the heated fluid rapidly moves away from the hot wall, and the thermal boundary layer thickness increases. Thus, the heat transfer performance (Nusselt number) decreases.

Figure 5 shows the average Nusselt number on the left wall of the enclosure as a function of the nanoparticle volume fraction for different values of the Rayleigh number Ra_{nf} and side wall angle θ. As the nanoparticle volume fraction increases from 0 to 2%, the Nusselt number decreases rapidly; as φ further increases from 2 to 4%, the average Nusselt number increases, but with a lower rate. The reasons for this behavior can be stated as follows. As the nanoparticle volume fraction increases, the viscosity of the mixture fluid increases. Therefore, the circulation capability near the walls falls down, and this event can decrease the heat transfer rate. However, with a further increase in the nanoparticle volume fraction above 2%, the increment of the thermal conductivity of the nanofluid could overcome the fluid circulation reduction; consequently, the Nusselt number gradually increases.

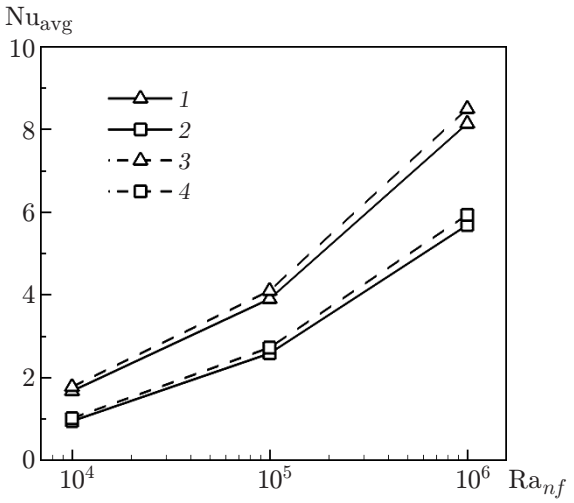

Fig. 3.

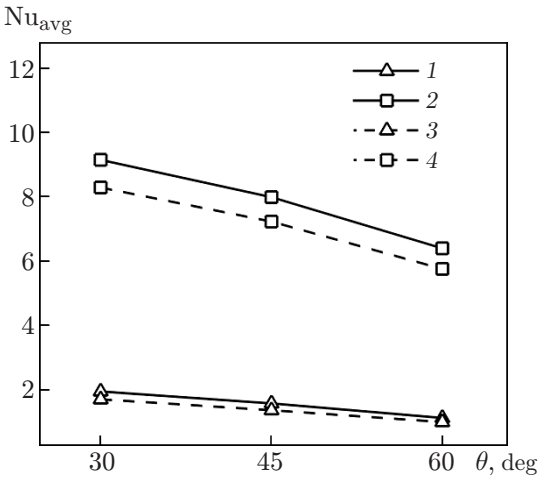

Fig. 4.

Fig. 3. Average Nusselt number on the left wall of the 2D enclosure versus the Rayleigh number for different side wall angles and nanoparticle volume fractions: (*1*) $\varphi = 2\%$ and $\theta = 30^\circ$; (*2*) $\varphi = 2\%$ and $\theta = 60^\circ$; (*3*) $\varphi = 4\%$ and $\theta = 30^\circ$; (*4*) $\varphi = 4\%$ and $\theta = 60^\circ$.

Fig. 4. Average Nusselt number on the left wall of the 2D enclosure versus the angle θ for different Rayleigh numbers and nanoparticle volume fractions: (*1*) $\varphi = 1\%$ and $\mathrm{Ra}_{nf} = 10^4$; (*2*) $\varphi = 3\%$ and $\mathrm{Ra}_{nf} = 10^4$; (*3*) $\varphi = 1\%$ and $\mathrm{Ra}_{nf} = 10^6$; (*4*) $\varphi = 3\%$ and $\mathrm{Ra}_{nf} = 10^6$.

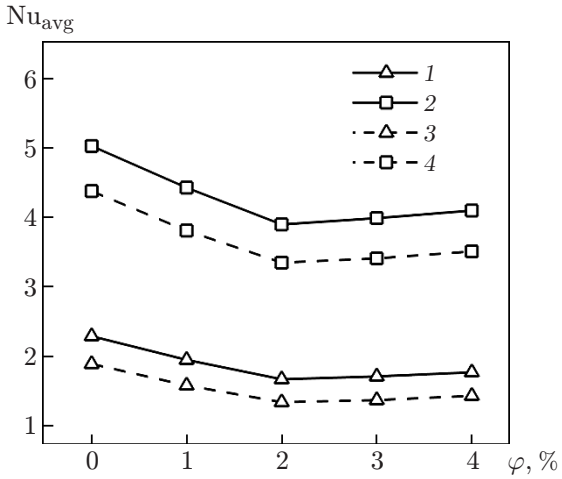

Fig. 5. Average Nusselt number on the left wall of the 2D enclosure versus the nanoparticle volume fraction for different Rayleigh numbers and side wall angles: (*1*) $\theta = 30^\circ$ and $\mathrm{Ra}_{nf} = 10^4$; (*2*) $\theta = 30^\circ$ and $\mathrm{Ra}_{nf} = 10^5$; (*3*) $\theta = 45^\circ$ and $\mathrm{Ra}_{nf} = 10^4$; (*4*) $\theta = 45^\circ$ and $\mathrm{Ra}_{nf} = 10^5$.

4.2. 3D Enclosure

Let us study natural convection of a nanofluid inside an inclined 3D channel with a trapezoidal cross section. The right and left side walls are kept at cold and hot temperatures, respectively; the top and bottom walls are subjected to an adiabatic condition. Periodic boundary conditions are imposed on the rear and front faces. In 3D problems, it is necessary to modify the characteristic length by $h = H/\cos\gamma$. Therefore, the Rayleigh number for

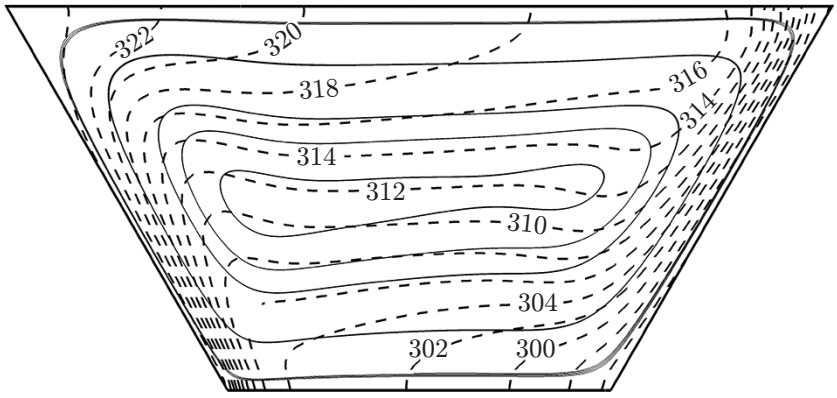

Fig. 6. Streamlines (solid curves) and isotherms (in Kelvin degrees) (dashed curves) in the 3D enclosure with a trapezoidal cross section for $\mathrm{Ra}_{nf,\gamma} = 10^5$, $\gamma = 30^\circ$, and $\varphi = 2\%$.

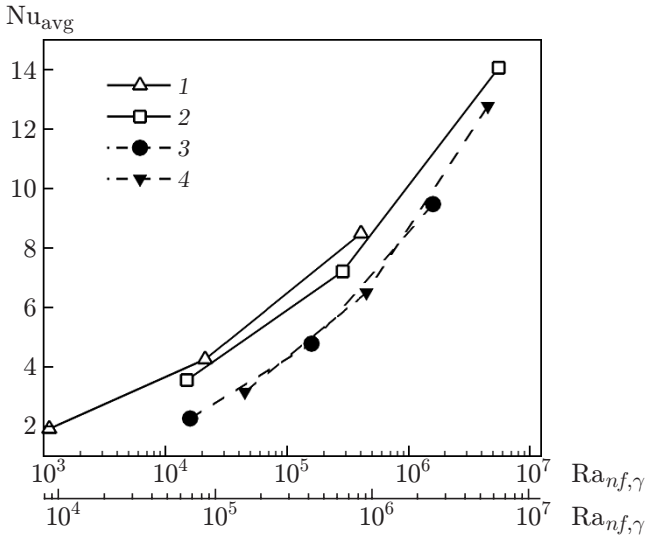

Fig. 7. Average Nusselt number on the left wall of the 3D enclosure versus the Rayleigh number (the lower and upper axes $\mathrm{Ra}_{nf,\gamma}$ refer to points 1,2 and 3,4, respectively) for different tilt angles and nanoparticle volume fractions: (*1*) $\varphi = 1\%$ and $\gamma = 10^\circ$; (*2*) $\varphi = 1\%$ and $\gamma = 60^\circ$; (*3*) $\varphi = 4\%$ and $\gamma = 10^\circ$; (*4*) $\varphi = 4\%$ and $\gamma = 60^\circ$.

3D problems is calculated by the formula $\mathrm{Ra}_{nf,\gamma} = g\beta_{nf}\Delta T H^3/(\alpha_{nf}\nu_{nf}\cos^3\gamma)$. Figure 6 shows the streamlines and isothermal lines of the flow for $\mathrm{Ra}_{nf,\gamma} = 10^5$, $\gamma = 30^\circ$, and $\varphi = 2\%$. The streamlines reveal intense fluid circulation inside the enclosure without producing small secondary vortices in the corners. The angle between the isotherms (in Kelvin degrees) and horizontal walls is 90°, and the temperature corresponding to these isotherms is equal to the temperature of the horizontal walls, which testifies to accurate boundary condition settings.

The effect of the Rayleigh number $\mathrm{Ra}_{nf,\gamma}$ on the average Nusselt number on the left side wall is illustrated in Fig. 7 for different values of the tilt angle γ and nanoparticle volume fraction φ. As the Rayleigh number increases, the average Nusselt number on the hot wall also increases for all values of γ and φ. This behavior is explained in Section 4.1 for the 2D enclosure.

The effect of the tilt angle γ on the average Nusselt number is illustrated for different values of the Rayleigh number Ra_{nf} and nanoparticle volume fraction φ. An increase in γ is accompanied by significant enhancement of the heat transfer intensity (Nusselt number). An increase in γ also leads to an increase in the characteristic length of the 3D channel ($h = H/\cos\gamma$). Therefore, according to Eq. (3), the Rayleigh number $\mathrm{Ra}_{nf,\gamma}$ and the thermal boundary layer thickness increase; consequently, the heat transfer enhancement is observed.

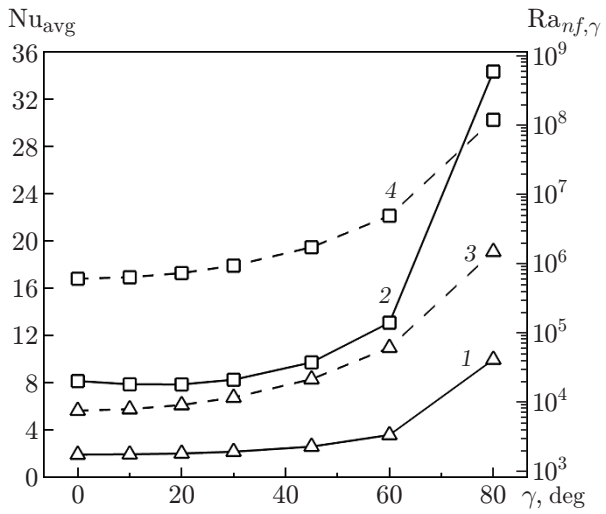

Fig. 8.

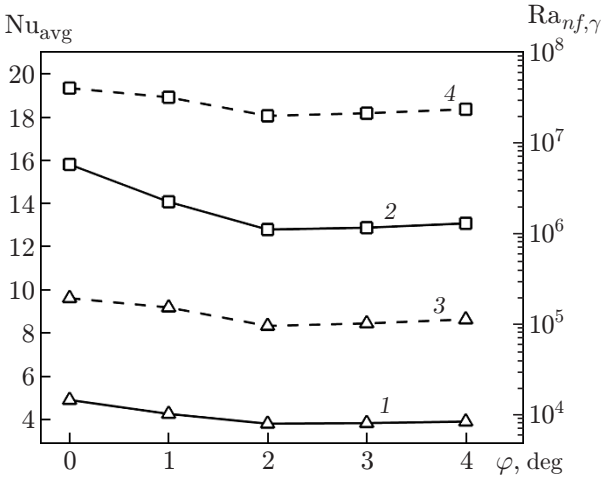

Fig. 9.

Fig. 8. Average Nusselt number (*1* and *2*) and Rayleigh number $\mathrm{Ra}_{nf,\gamma}$ (*3* and *4*) on the left wall versus the tilt angle for different values of the Rayleigh number and nanoparticle volume fraction: (*1*) $\mathrm{Ra}_{nf} = 10^4$ and $\varphi = 1\%$; (*2*) $\mathrm{Ra}_{nf} = 10^4$ and $\varphi = 4\%$; (*3*) $\mathrm{Ra}_{nf} = 10^6$ and $\varphi = 1\%$; (*4*) $\mathrm{Ra}_{nf} = 10^6$ and $\varphi = 4\%$.

Fig. 9. Average Nusselt number (*1* and *2*) and Rayleigh number $\mathrm{Ra}_{nf,\gamma}$ (*3* and *4*) on the left wall of the enclosure versus the nanoparticle volume fraction for different values of the Rayleigh number and tilt angle: (*1*) $\mathrm{Ra}_{nf} = 10^5$ and $\gamma = 10^\circ$; (*2*) $\mathrm{Ra}_{nf} = 10^5$ and $\gamma = 60^\circ$; (*3*) $\mathrm{Ra}_{nf} = 10^6$ and $\gamma = 10^\circ$; (*4*) $\mathrm{Ra}_{nf} = 10^6$ and $\gamma = 60^\circ$.

Figure 9 shows the average Nusselt number as a function of the volume fraction of Al_2O_3 nanoparticles for different values of the Rayleigh number and tilt angle of the enclosure. As the nanoparticle volume fraction increases from 0 to 2%, the Nusselt number decreases rapidly; with a further increase in the nanoparticle volume fraction from 2% to 4%, the Nusselt number increases with a lower rate. This behavior can be explained as follows. As the nanoparticle volume fraction increases, the nanofluid viscosity also increases. Therefore, the fluid circulation capability near the hot walls falls down, resulting in reduction of the heat transfer rate. However, with a further increase in the nanoparticle volume fraction above 2%, the increment of the thermal conductivity of the nanofluid could compensate for circulation reduction; consequently, the Nusselt number gradually increases.

CONCLUSIONS

Heat transfer due to free convection of a nanofluid with variable properties in 2D and 3D channels with trapezoidal cross sections is investigated in the present study. The governing equations are solved numerically by using the finite volume method and the SIMPLER algorithm. The effects of the nanoparticle volume fraction, Rayleigh number, and side wall angle on heat transfer performance are considered. For both 2D and 3D enclosures, an increment of the Rayleigh number is accompanied by enhancement of natural convection heat transfer. As the nanoparticle volume fraction increases from 0 to 2%, a rapid decrease in the Nusselt number is observed; however, a further increase in the nanoparticle volume fraction from 2 to 4% leads to an increase in the Nusselt number, but with a slower rate. Furthermore, an increase in the side wall angle leads to a decrease in the Nusselt number in 2D enclosures and to its increase in 3D enclosures.

The authors would like to acknowledge the Shahrood University of Technology, which supported this project.

REFERENCES

1. V. Karthik, S. Sahoo, S. K. Pabi, and S. Ghosh, "On the Phononic and Electronic Contribution to the Enhanced Thermal Conductivity of Water-Based Silver Nanofluids," Int. J. Thermal Sci. **64**, 53–61 (2013).
2. K. V. Wong and O. De Leon, "Applications of Nanofluids: Current and Future," Adv. Mech. Eng. **2**, 519659 (2010).
3. R. Saidur, K. Y. Leong, and H. A. Mohammad, "A Review on Applications and Challenges of Nanofluids," Renewable Sustainable Energy Rev. **15** (3), 1646–1668 (2011).
4. D. Yadav, C. Kim, J. Lee, and H. H. Cho, "Influence of Magnetic Field on the Onset of Nanofluid Convection Induced by Purely Internal Heating," Comput. Fluids **121**, 26–36 (2015).
5. D. Wen and Y. Ding, "Experimental Investigation into Convective Heat Transfer of Nanofluids at the Entrance Region under Laminar Flow Conditions," Int. J. Heat Mass Transfer **47** (24), 5181–5188 (2004).
6. S. M. Aminossadati and B. Ghasemi, "Natural Convection Cooling of a Localised Heat Source at the Bottom of a Nanofluid-Filled Enclosure," Europ. J. Mech. B. Fluids **28** (5), 630–640 (2009).
7. S. M. Aminossadati and B. Ghasemi, "Enhanced Natural Convection in an Isosceles Triangular Enclosure Filled with a Nanofluid," Comput. Math. Appl. **61** (7), 1739–1753 (2011).
8. R. Y. Jou and S. C. Tzeng, "Numerical Research of Nature Convective Heat Transfer Enhancement Filled with Nanofluids in Rectangular Enclosures," Int. Comm. Heat Mass Transfer **33** (6), 727–736 (2006).
9. K. Khanafer, K. Vafai, and M. Lightstone, "Buoyancy-Driven Heat Transfer Enhancement in a Two-Dimensional Enclosure Utilizing Nanofluids," Int. J. Heat Mass Transfer **46** (19), 3639–3653 (2003).
10. M. Saidi and G. Karimi, "Free Convection Cooling in Modified L-Shape Enclosures Using Copper–Water Nanofluid," Energy **70**, 251–271 (2014).
11. M. Sheikholeslami, M. Gorji-Bandpay, and D. D. Ganji, "Magnetic Field Effects on Natural Convection around a Horizontal Circular Cylinder Inside a Square Enclosure Filled with Nanofluid," Int. Comm. Heat Mass Transfer **39** (7), 978–986 (2012).
12. S. M. Sebdani, M. Mahmoodi, and S. M. Hashemi, "Effect of Nanofluid Variable Properties on Mixed Convection in a Square Cavity," Int. J. Thermal Sci. **52**, 112–126 (2012).
13. M. Sheikholeslami, M. Gorji-Bandpy, D. D. Ganji, et al., "Natural Convection of Nanofluids in an Enclosure between a Circular and a Sinusoidal Cylinder in the Presence of Magnetic Field," Int. Comm. Heat Mass Transfer **39** (9), 1435–1443 (2012).
14. R. Roslan, H. Saleh, and I. Hashim, "Effect of Rotating Cylinder on Heat Transfer in a Square Enclosure Filled with Nanofluids," Int. J. Heat Mass Transfer **55** (23), 7247–7256 (2012).
15. S. H. Hussain and A. K. Hussein, "Mixed Convection Heat Transfer in a Differentially Heated Square Enclosure with a Conductive Rotating Circular Cylinder at Different Vertical Locations," Int. Comm. Heat Mass Transfer **38** (2), 263–274 (2011).
16. N. Putra, W. Roetzel, and S. K. Das, "Natural Convection of Nano-Fluids," Heat Mass Transfer **39** (8/9), 775–784 (2003).
17. E. B. Öğüt, "Natural Convection of Water-Based Nanofluids in an Inclined Enclosure with a Heat Source," Int. J. Thermal Sci. **48** (11), 2063–2073 (2009).
18. Y. Hu, Y. He, C. Qi, et al., "Experimental and Numerical Study of Natural Convection in a Square Enclosure Filled with Nanofluid," Int. J. Heat Mass Transfer **78**, 380–392 (2014).
19. Y. Hu, Y. He, S. Wang, et al., "Experimental and Numerical Investigation on Natural Convection Heat Transfer of TiO_2–Water Nanofluids in a Square Enclosure," J. Heat Transfer **136** (2), 022502 (2014).
20. M. Corcione, M. Cianfrini, and A. Quintino, "Enhanced Natural Convection Heat Transfer of Nanofluids in Enclosures with Two Adjacent Walls Heated and the Two Opposite Walls Cooled," Int. J. Heat Mass Transfer **88**, 902–913 (2015).
21. M. Bouhalleb and H. Abbassi, "Natural Convection of Nanofluids in Enclosures with Low Aspect Ratios," Int. J. Hydrogen Energy **39** (27), 15275–15286 (2014).
22. M. N. Hasan, K. Samiuzzaman, S. H. Haque, et al., "Mixed Convection Heat Transfer Inside a Square Cavity Filled with Cu–Water Nanofluid," Procedia Eng. **105**, 438–445 (2015).
23. H. Saleh, R. Roslan, and I. Hashim, "Natural Convection Heat Transfer in a Nanofluid-Filled Trapezoidal Enclosure," Int. J. Heat Mass Transfer **54** (1), 194–201 (2011).
24. M. H. Esfe, A. A. A. Arani, W. M. Yan, et al., "Natural Convection in a Trapezoidal Enclosure Filled with Carbon Nanotube–EG–Water Nanofluid," Int. J. Heat Mass Transfer **92**, 76–82 (2016).

25. M. A. Sheremet, T. Groşan, and I. Pop, "Steady-State Free Convection in Right-Angle Porous Trapezoidal Cavity Filled by a Nanofluid: Buongiorno's Mathematical Model," Europ. J. Mech. B. Fluids **53**, 241–250 (2015).
26. M. H. Hasib, M. S. Hossen, and S. Saha, "Effect of Tilt Angle on Pure Mixed Convection Flow in Trapezoidal Cavities Filled with Water–Al_2O_3 Nanofluid," Procedia Eng. **105**, 388–397 (2015).
27. R. Nasrin and S. Parvin, "Investigation of Buoyancy-Driven Flow and Heat Transfer in a Trapezoidal Cavity Filled with Water–Cu Nanofluid," Int. Comm. Heat Mass Transfer **39** (2), 270–274 (2012).
28. A. H. Mahmoudi, I. Pop, M. Shahi, and F. Talebi, "MHD Natural Convection and Entropy Generation in a Trapezoidal Enclosure Using Cu–Water Nanofluid," Comput. Fluids **72**, 46–62 (2013).
29. E. Abu-Nada, "Effects of Variable Viscosity and Thermal Conductivity of Al_2O_3–Water Nanofluid on Heat Transfer Enhancement in Natural Convection," Int. J. Heat Fluid Flow **30** (4), 679–690 (2009).
30. S. P. Jang and S. U. Choi, "Effects of Various Parameters on Nanofluid Thermal Conductivity," J. Heat Transfer **129** (5), 617–623 (2007).
31. A. Arefmanesh, A. Aghaei, and H. Ehteram, "Mixed Convection Heat Transfer in a CuO–Water Filled Trapezoidal Enclosure, Effects of Various Constant and Variable Properties of the Nanofluid," Appl. Math. Modelling **40** (2), 815–831 (2016).
32. E. Abu-Nada, Z. Masoud, H. F. Oztop, and A. Campo, "Effect of Nanofluid Variable Properties on Natural Convection in Enclosures," Int. J. Thermal Sci. **49** (3), 479–491 (2010).
33. C. T. Nguyen, F. Desgranges, G. Roy, et al., "Temperature and Particle-Size Dependent Viscosity Data for Water-Based Nanofluids—Hysteresis Phenomenon," Int. J. Heat Fluid Flow **28** (6), 1492–1506 (2007).
34. W. Yu and S. U. S. Choi, "The Role of Interfacial Layers in the Enhanced Thermal Conductivity of Nanofluids: A Renovated Maxwell Model," J. Nanoparticle Res. **5** (1/2), 167–171 (2003).
35. Q. Z. Xue, "Model for Effective Thermal Conductivity of Nanofluids," Phys. Lett. A **307** (5), 313–317 (2003).
36. C. H. Chon, K. D. Kihm, S. P. Lee, and S. U. Choi, "Empirical Correlation Finding the Role of Temperature and Particle Size for Nanofluid (Al_2O_3) Thermal Conductivity Enhancement," Appl. Phys. Lett. **87** (15), 3107 (2005).
37. S. V. Patankar, *Numerical Heat Transfer and Fluid Flow* (Hemisphere–Taylor and Francis Group, New York, 1980).
38. H. K. Versteeg and W. Malalasekera, *An Introduction to Computational Fluid Dynamic: The Finite Volume Method* (John Wiley, New York, 1995).
39. R. J. Krane and J. Jessee, "Some Detailed Field Measurements for a Natural Convection Flow in a Vertical Square Enclosure," in *Proc. 1st ASME–JSME Thermal Eng. Joint Conf., 1983*, Vol. 1, pp. 323–329.